

Resonant-amplified and invisible Bragg scattering based on spin coalescing modes

K. L. Zhang and Z. Song*

School of Physics, Nankai University, Tianjin 300071, China

(Dated: July 19, 2022)

Unlike a real magnetic field, which separates the energy levels of particle with opposite spin polarization, a complex field can lead to a special kind of spectral degeneracy, known as exceptional point (EP), at which two spin eigenmodes coalesce. It allows an EP impurity to be an invisible scattering center for a fermion with the resonant spin polarization, but an amplifying emitter for opposite polarization. We show that a pair of conjugate EP modes supports resonant mutual stimulation, acting as a resonant amplifier based on the underlying mechanism of positive-feedback loop. Together with other Hermitian eigenmodes, a fermion with EP polarization exhibits some exclusive dynamics, referred to as EP dynamics. We construct several typical superlattices, which are built up by embedding EP-impurity arrays in Hermitian two-dimensional square lattice. Numerical simulations are performed to demonstrate resonant amplification and invisibility of Bragg fringe.

I. INTRODUCTION

Spin as an intrinsic degree of freedom of a particle, is the origin of magnetism and is a fundamental property of particles, which is employed in spintronics¹ for information processing. Carrying information in both the spin and charge of a particle potentially offers devices with a greater diversity of functionality. In a real magnetic field two energy levels of a half spin is separated, associating with the spin can either be aligned along the field, or against the field. Then a particle with arbitrary spin polarization is unavoidably scattered by a magnetic impurity defined as Zeeman term $\mathbf{B} \cdot \mathbf{s}$, where \mathbf{s} is a spin operator at local magnetic field \mathbf{B} . However, in stark contrast, an imaginary component of \mathbf{B} field can shrink the energy gap between two opposite spin states. Remarkably, the gap can be tuned to vanish, resulting the coalescence of two spin states. It relates to an exclusive concept in a non-Hermitian system, exceptional point (EP), which has no counterpart in a Hermitian system. We refer such an impurity to as EP impurity. The EP in a non-Hermitian system occurs when eigenstates coalesce²⁻⁴, and usually associates with the non-Hermitian phase transition^{5,6}. In a parity-time (\mathcal{PT}) symmetric non-Hermitian coupled system, the \mathcal{PT} symmetry of eigenstates spontaneously breaks at the EP⁷⁻¹⁷, which determines the exact \mathcal{PT} -symmetric phase and the broken \mathcal{PT} -symmetric phase in this system.

The EP has many applications in optics^{15,18-23}, not limited to non-reciprocal energy transfer²⁰, unidirectional lasing^{24,25}, and optical sensing^{26,27}. Moreover, the EP is a bifurcation point of the energy levels. Near the EP, the eigen frequency response to the perturbation exhibits a square-root dependence²⁶ and a cubic-root²⁷ dependence, respectively. In this regard, the EPs are useful for sensing in comparison with the diabolic points; this feature has been verified in optics, cavity optomechanics, cavity spintronics, and circuit quantum electrodynamics²⁸⁻³⁷. The sensing susceptibility is greatly enhanced near the EPs³⁸.

In addition to this, the dynamics of the systems with parameters far away from, near and at the EP, exhibit ex-

tremely different behaviors³⁹⁻⁴¹. When system $\mathbf{B} \cdot \mathbf{s}$ is far from or near EP but with finite energy gap, the dynamics is a periodic oscillation with associated Dirac probability oscillating in the period of time inversely proportional to the gap. When system is at EP, the Dirac probability may be constant or increase quadratically with time, i.e., the EP dynamics of the spin strongly depends on the initial state. This raises interesting questions regarding the non-Hermitian spintronics based on particular EP-related dynamics of electrons. Importantly, complex magnetic field is no longer a component of a toy model, but has been investigated in a practice perspective⁴².

In this paper, we investigate the effect of EP impurity on a particle wave propagating in the Hermitian lattice in which various EP impurity arrays are embedded. The EP dynamics allows an EP impurity to be an invisible scattering center for a particle with the resonant spin polarization, but an amplifying emitter for opposite polarization. We show that a pair of conjugate EP modes supports resonant mutual stimulation, acting as a resonant amplifier based on the underlying mechanism of positive-feedback loop. The important points are that (i) one of the two conjugate EP modes is the auxiliary mode to another, i.e., mutual auxiliary states and (ii) two conjugate EP modes are orthogonal in the context of Dirac inner product. Together with other Hermitian eigenmodes that can be represented as two conjugate EP modes, a particle with EP polarization exhibits some exclusive dynamics, referred to as EP dynamics. We construct several typical superlattices, which are built up by embedding EP-impurity array in Hermitian two-dimensional (2D) square lattice. Numerical simulations are performed to demonstrate resonant amplification and invisibility of Bragg fringe.

This paper is organized as follows. In Sec. II, we introduce a non-Hermitian spin- $\frac{1}{2}$ fermionic model and discuss the coalescing spin modes. In Sec. III, we analyse the mechanism of positive-feedback loop through a exactly solvable 1D model. In Sec. IV, we demonstrate the dynamics of resonant amplification and invisibility of Bragg fringe in 2D square lattices. Finally, we summarize our results in Sec. V.

II. HAMILTONIAN AND COALESCING SPIN MODES

We begin this section by introducing a non-interacting spin- $\frac{1}{2}$ fermionic model with complex impurities, which arise the non-Hermiticity of the Hamiltonian. We will show that it supports intriguing dynamic behavior since it is a concrete example of a class of non-Hermitian Hamiltonian presented in the Appendix. The Hamiltonian on an arbitrary lattice can be written as

$$H = \sum_{j < l} \sum_{\sigma=\uparrow,\downarrow} \kappa_{jl} c_{j,\sigma}^\dagger c_{l,\sigma} + \text{H.c.} + \sum_j \mathbf{B}_j \cdot \mathbf{s}_j, \quad (1)$$

where operator $c_{j,\sigma}^\dagger$ creates a fermion of spin σ at site j , and $\mathbf{s}_j = (s_j^x, s_j^y, s_j^z)$ is the spin- $\frac{1}{2}$ operator, which is defined by $s_j^\alpha = \frac{1}{2} c_j^\dagger \tau^\alpha c_j$, satisfying the Lie algebra commutation relation

$$[s_j^\alpha, s_j^\beta] = \sum_{\gamma=x,y,z} i\epsilon^{\alpha\beta\gamma} s_j^\gamma, \quad (2)$$

and τ^α ($\alpha = x, y, z$) are the Pauli matrices; c_j^\dagger is defined as $c_j^\dagger = (c_{j,\uparrow}^\dagger, c_{j,\downarrow}^\dagger)$; and $\epsilon^{\alpha\beta\gamma}$ is the Levi-Civita symbol. Here κ_{jl} is hopping strength between two sites j and l , determining the geometry of the lattice, and \mathbf{B}_j is on-site complex magnetic field, inducing non-Hermitian impurity. In this work, we only consider three types of sites with

$$\mathbf{B}_j = |B_j| \begin{cases} 0 \\ (1, 0, i) \\ (1, 0, -i) \end{cases}, \quad (3)$$

respectively.

The crucial point is that there are two types of EPs for terms $\mathbf{B}_j \cdot \mathbf{s}_j$ with nonzero $|B_j|$. We note that two types of EP-impurities possess two different coalescing spin modes $\frac{1}{\sqrt{2}} (c_{j,\uparrow}^\dagger \pm i c_{j,\downarrow}^\dagger) |\text{Vac}\rangle$, i.e., under the basis $(c_{j,\uparrow}^\dagger |\text{Vac}\rangle, c_{j,\downarrow}^\dagger |\text{Vac}\rangle)$, we have

$$\frac{1}{2} |B_j| \begin{pmatrix} \pm i & 1 \\ 1 & \mp i \end{pmatrix} \begin{pmatrix} 1 \\ \mp i \end{pmatrix} = 0. \quad (4)$$

Interestingly, such two EP modes are mutually auxiliary modes to each other, respectively, i.e.,

$$\frac{1}{2} |B_j| \begin{pmatrix} \pm i & 1 \\ 1 & \mp i \end{pmatrix} \begin{pmatrix} 1 \\ \pm i \end{pmatrix} = \pm i |B_j| \begin{pmatrix} 1 \\ \mp i \end{pmatrix}. \quad (5)$$

In addition, two EP modes are orthogonal in the context of Dirac inner product as two eigenmodes for term $\mathbf{B}_j \cdot \mathbf{s}_j$ with zero $|B_j|$.

The general feature of such a system obeys the conclusion presented in the Appendix, as an example with $N_{\text{clust}} = 2$. Accordingly, there are two types of dynamics in a system with only one type of EP-impurity: (i) When

only the EP mode is involved in an initial state, the Dirac probability is conservative. (ii) When only the auxiliary mode is involved in an initial state, the Dirac probability is not conservative. In this paper, we are interested in the case that there are two types of EP-impurities are embedded in the lattice, forming a special structure we dub it EP superlattice. Importantly, the relation of mutually auxiliary modes should result in mutual stimulation. We will demonstrate this point analytically and numerically in the following sections.

III. RESONANT MUTUAL STIMULATION

In this section, we investigate the probability amplification by resonant mutual stimulation based on a simple analysis for a system with two different EP-sites embedded. An EP-site can create probability with the auxiliary EP mode of another EP-site but remains the probability of initial state. As time being, it will result in a mutual stimulation. The total probability should be amplified definitely when the system is finite due to the reflection from the boundary.

We demonstrate the concept quantitatively by an exactly solvable model, which is an Hermitian chain with embedded two EP-sites at ends. There are two types of systems with the Hamiltonians

$$H_\pm = H_{\text{chain}} + \mathbf{B}_+ \cdot \mathbf{s}_1 + \mathbf{B}_\mp \cdot \mathbf{s}_N, \\ H_{\text{chain}} = \sum_{j=1}^{N-1} \sum_{\sigma=\uparrow,\downarrow} c_{j,\sigma}^\dagger c_{j+1,\sigma} + \text{H.c.}, \quad (6)$$

where the complex fields $\mathbf{B}_\pm = |B|(1, 0, \pm i)$. The two types of systems H_+ and H_- are schematically illustrated in Fig. 1(a). Applying the transformation

$$d_{j,\lambda} = \sqrt{\frac{\lambda}{2}} (c_{j,\uparrow} + \lambda i c_{j,\downarrow}), \quad (7)$$

with $\lambda = \pm$, we have the equivalent Hamiltonians

$$H_\pm = H_{\text{chain}} + |B| d_{1,+}^\dagger d_{1,-} + |B| d_{N,\mp}^\dagger d_{N,\pm}, \\ H_{\text{chain}} = \sum_{j=1}^{N-1} \sum_{\lambda=+,-} (d_{j,\lambda}^\dagger d_{j+1,\lambda} + d_{j+1,\lambda}^\dagger d_{j,\lambda}), \quad (8)$$

where operators $d_{j,\lambda}^\dagger$ and $d_{j,\lambda}$ satisfy the anti-commutation relations

$$\{d_{j,\lambda}, d_{j',\lambda'}^\dagger\} = \delta_{j,j'} \delta_{\lambda,\lambda'}, \\ \{d_{j,\lambda}, d_{j',\lambda'}\} = \{d_{j,\lambda}^\dagger, d_{j',\lambda'}^\dagger\} = 0. \quad (9)$$

The transformation in Eq. (7) is unitary, which is different from the similarity transformation in Eq. (A3) that block diagonalizes the original Hamiltonian (see Appendix 1). Here, the biorthogonal conjugation operator $\bar{d}_{j,\lambda}$ defined in the Appendix reduces to $d_{j,\lambda}^\dagger$ due to the

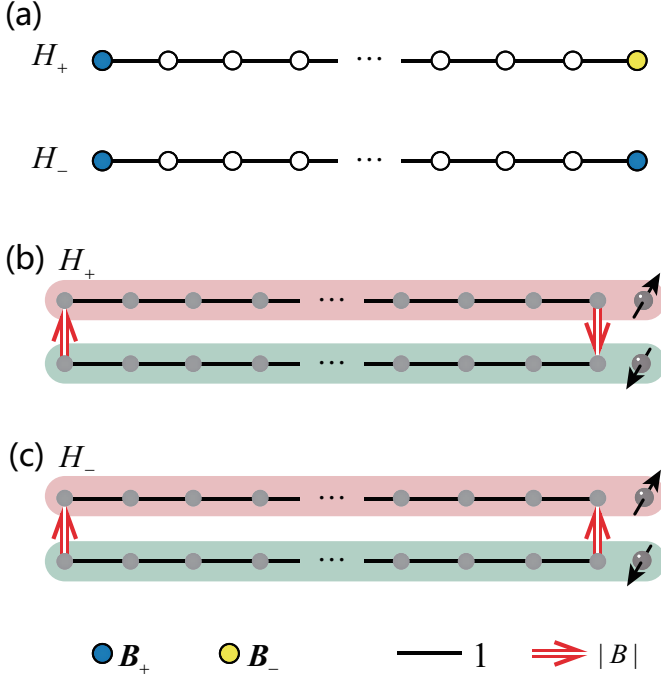


FIG. 1. Schematic illustrations for (a) Hamiltonian in Eq. (6), where the EP-sites with complex fields B_+ and B_- are represented by the blue and yellow dots, respectively. (b) Equivalent Hamiltonians for H_+ and (c) H_- in Eq. (8). Here the red arrow indicates that the systems support unidirectional transition between two types of spin polarizations, and H_+ act as a positive feedback loop.

fact that two EP modes are orthogonal in the context of Dirac inner product. We note that terms $|B| d_{1,+}^\dagger d_{1,-}$ and $|B| d_{N,\mp}^\dagger d_{N,\pm}$ represent unidirectional transitions between different spin polarizations. Such a transformation still holds for a general lattice with arbitrary geometry. Going back to the present example, we find that Hamiltonian H_+ and H_- are equivalent to two types of feedback loops (rings with two unidirectional dimmers), which are schematically illustrated in Fig. 1(b) and (c), respectively. In particular, Hamiltonian H_+ forms a positive-feedback loop that supports dynamics of mutual stimulation.

To understand the positive-feedback dynamics in such a system, we will explore the features of the asymmetric dimer, which can be applied to the original system in Eq. (8). We focus on a scattering problem for an asymmetry dimer which is embedded in an infinite chain. For simplicity, we consider the Hamiltonian in single-particle invariant subspace, which reads

$$H_{\text{scatt}} = \sum_{j=1}^{\infty} (|j\rangle \langle j+1| + |-j\rangle \langle -j-1|) + \text{H.c.} + \mu |1\rangle \langle -1| + \nu |-1\rangle \langle 1|. \quad (10)$$

Here position state $|\lambda j\rangle = d_{j,\lambda}^\dagger |\text{Vac}\rangle$ with $|\text{Vac}\rangle$ being vacuum state of operators $c_{j,\uparrow}$ and $c_{j,\downarrow}$. Parameters (μ, ν)

are asymmetric hopping amplitudes, exhibiting the feature of asymmetric transmission in a simple way. The Bethe ansatz scattering solution assumes the form

$$|\psi_k\rangle = \sum_{j=1}^{\infty} [f_k(j) |j\rangle + f_k(-j) |-j\rangle] \quad (11)$$

where the wave function $f_k(j)$ reads

$$f_k(j) = \begin{cases} e^{ikj} + r_k e^{-ikj}, & j \leq -1 \\ t_k e^{ikj}, & j \geq 1 \end{cases}. \quad (12)$$

Here r_k and t_k are the reflection and transmission amplitudes of the incident wave with momentum k , which can be used to characterize the property of the dimer. It is the solution for an incident wave from left of the system. Similarly, the solution for an incident wave from right can be obtained by exchanging ν and μ . By solving the Schrödinger equation $H_{\text{scatt}} |\psi_k\rangle = E_k |\psi_k\rangle$, we obtain

$$r_k = \frac{1 - \mu\nu}{\mu\nu e^{2ik} - 1}, \quad t_k = \frac{2i\mu \sin k}{\mu\nu e^{2ik} - 1}. \quad (13)$$

The result can be applied to the model in Eq. (8) by taking $(\mu, \nu) = (|B|, 0)$ or $(0, |B|)$, representing the dynamics for two types of initial state with spin polarizations $\lambda = \pm$, respectively. (i) For $(\mu, \nu) = (|B|, 0)$, we have $|r_k| = 1$ and $|t_k| = 2|B| \sin k$, (ii) while $|r_k| = 1$ and $|t_k| = 0$, for $(\mu, \nu) = (0, |B|)$. It indicates that we always have $|r_k| = 1$ in both cases.

Next, we further uncover and verify the above mechanism by considering the process of a spin polarized Gaussian wave packet being scattered by the right ends of chains H_+ and H_- , numerically. The initial excitation is taken as $|\psi(0)\rangle = (\alpha/\sqrt{\pi})^{1/2} \sum_{j=1}^N e^{-\alpha^2(j-j^c)^2/2} e^{ik^c j} d_{j,+}^\dagger |\text{Vac}\rangle$, where j^c is the center of wave packet; k^c is the central momentum; and α characterizes the width. The site state $d_{j,+}^\dagger |\text{Vac}\rangle$ is auxiliary mode of term $B_- \cdot \mathbf{s}_j$ and EP mode of term $B_+ \cdot \mathbf{s}_j$. The evolved state can be represented in the form $|\psi_\pm(t)\rangle = e^{-iH_\pm t} |\psi(0)\rangle$, which can be computed by exact diagonalization numerically. To monitor the evolved state, we introduce the overlap between evolved state and polarized state $|k, \lambda\rangle = (1/\sqrt{N}) \sum_{j=1}^N e^{ikj} d_{j,\lambda}^\dagger |\text{Vac}\rangle$ in momentum space

$$F_\pm^\lambda(k, t) = |\langle k, \lambda | \psi_\pm(t) \rangle| \quad (14)$$

where $k = 2\pi m/N$ (m is an integer in interval $(-N/2, N/2]$), and $\lambda = \pm$. Overlap $F_\pm^\lambda(k, t)$ characterizes the component of evolved state $|\psi_\pm(t)\rangle$. That is, $F_\pm^+(k, t)$ and $F_\pm^-(k, t)$ count the same and different spin polarizations as the initial excitation, respectively, as function of momentum k and time t . In other words, nonzero $F_\pm^\lambda(k, t)$ will reflect the emergence of spin-orbit effect. In the right panel of Fig. 2, we plot $F_\pm^\lambda(k, t)$ obtained from exact diagonalization numerically. It indicates that the evolved state in system H_+ has evident spin-orbit effect [see Fig. 2(a)] and evolved state in system H_- has no spin-orbit effect [see Fig. 2(b)].

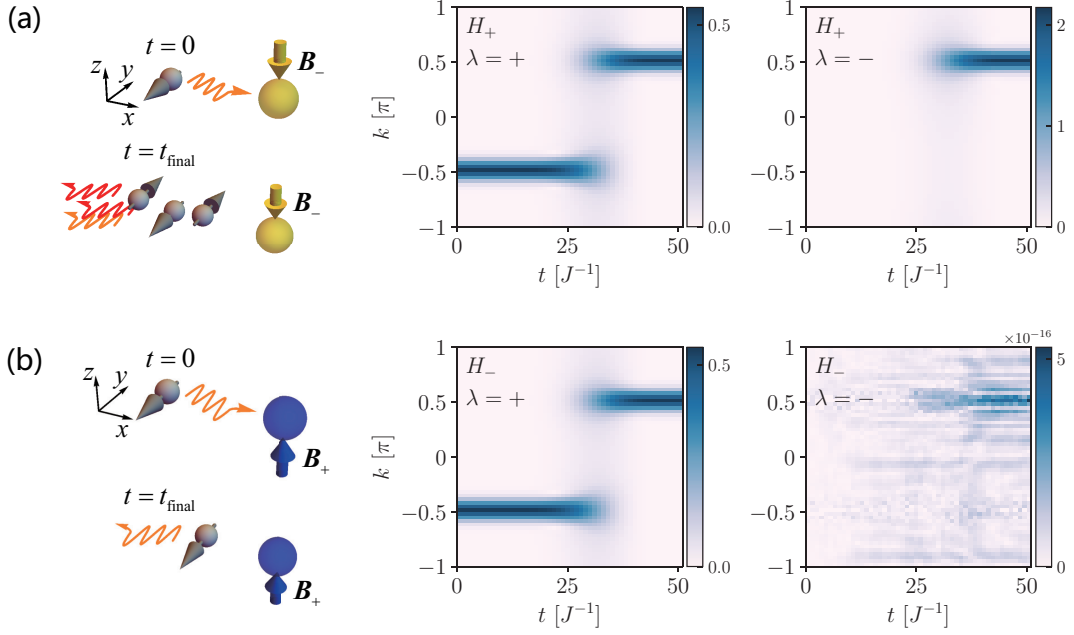


FIG. 2. Spin-orbit effect in the scattering process. The left panels of (a) and (b) are the schematic illustrations of the processes in systems H_+ and H_- , respectively. The yellow (blue) arrow represents local complex field \mathbf{B}_- (\mathbf{B}_+). Correspondingly, numerical result of the overlap $F_\pm^\lambda(k, t)$ defined in Eq. (14) is present in the right panels of (a) $F_+^\lambda(k, t)$ and (b) $F_-^\lambda(k, t)$. It indicates that after being scattered by the complex fields, the spin polarization of initial excitation is conservative in both systems; and for system H_+ , the outgoing wave packet contains the other spin polarization (which is zero for system H_-). The parameters of initial excitation are $\alpha = 0.2$, $j^c = 30$ and $k^c = -\pi/2$, and are $|B| = 1$ and $N = 60$ for the both systems. Here the scale of the Hamiltonian is $J = 2$.

It provides a clear physical picture for understanding the feedback dynamics of H_\pm . (i) For system H_+ , any initial wave packet (except the plane wave with $k = 0$ and π) can trigger the Dirac probability explosion since the EP modes at the ends of chain are mutual auxiliary modes. The underlying mechanism is mutual stimulation. In addition, the evolved state has evident spin-orbit effect. The momentum and spin polarization of a particle are strongly correlated. (ii) For system H_- , the result depends on the initial state: (a) For initial wave packet with EP mode, the probability is conservative, since there is no mode switch. In contrast, the evolved state has no spin-orbit effect. (b) For initial wave packet with auxiliary EP mode, the probability with auxiliary EP mode is conservative, while the probability with EP mode increases since there is always particle with auxiliary EP mode can provide the source to the probability with EP mode. And as time being, probability with EP mode is dominant. We would like to point out that this amplification is fragile since it depends on the conservation of probability with auxiliary EP mode. When a 2D lattice is considered, the probability with EP mode spreads and cannot supply the switch to the probability with EP mode.

IV. AMPLIFIED BRAGG FRINGE

Now we extend our investigation to the 2D systems which support dynamics of Bragg scattering. We consider a specific form of Hamiltonian Eq. (1), wherein the EP-impurity array as superlattice is embedded in a Hermitian $N_x \times N_y$ square lattice with uniform nearest-neighbor hopping κ . We will focus on four configurations of the superlattices composed of two parallel EP-impurity arrays, in which, dynamics of invisible Bragg scattering, amplified Bragg scattering, and resonant mutual stimulation can be realized.

As a comparison and warm up, let us first consider the dynamics of Bragg scattering in a Hermitian system with two parallel arrays formed by real magnetic field $\mathbf{B} = (|B|, 0, 0)$ (marked by gray circles in Fig. 3). The initial excitation is an incident wave packet with a fixed spin polarization

$$|\Psi(0)\rangle = \frac{1}{\sqrt{2\Omega}} \sum_{j=1}^{N_x} \sum_{l=1}^{N_y} e^{-\alpha^2[(j-j^c)^2 + (l-l^c)^2]/2} e^{i(k_x^c j + k_y^c l)} \times (c_{j,l,\uparrow}^\dagger - i c_{j,l,\downarrow}^\dagger) |\text{Vac}\rangle, \quad (15)$$

where $\Omega = \sum_{j,l} e^{-\alpha^2[(j-j^c)^2 + (l-l^c)^2]}$ is the Dirac normalization factor; j and l are site indexes of the lattice in x and y directions; (j^c, l^c) is the center of wave packet

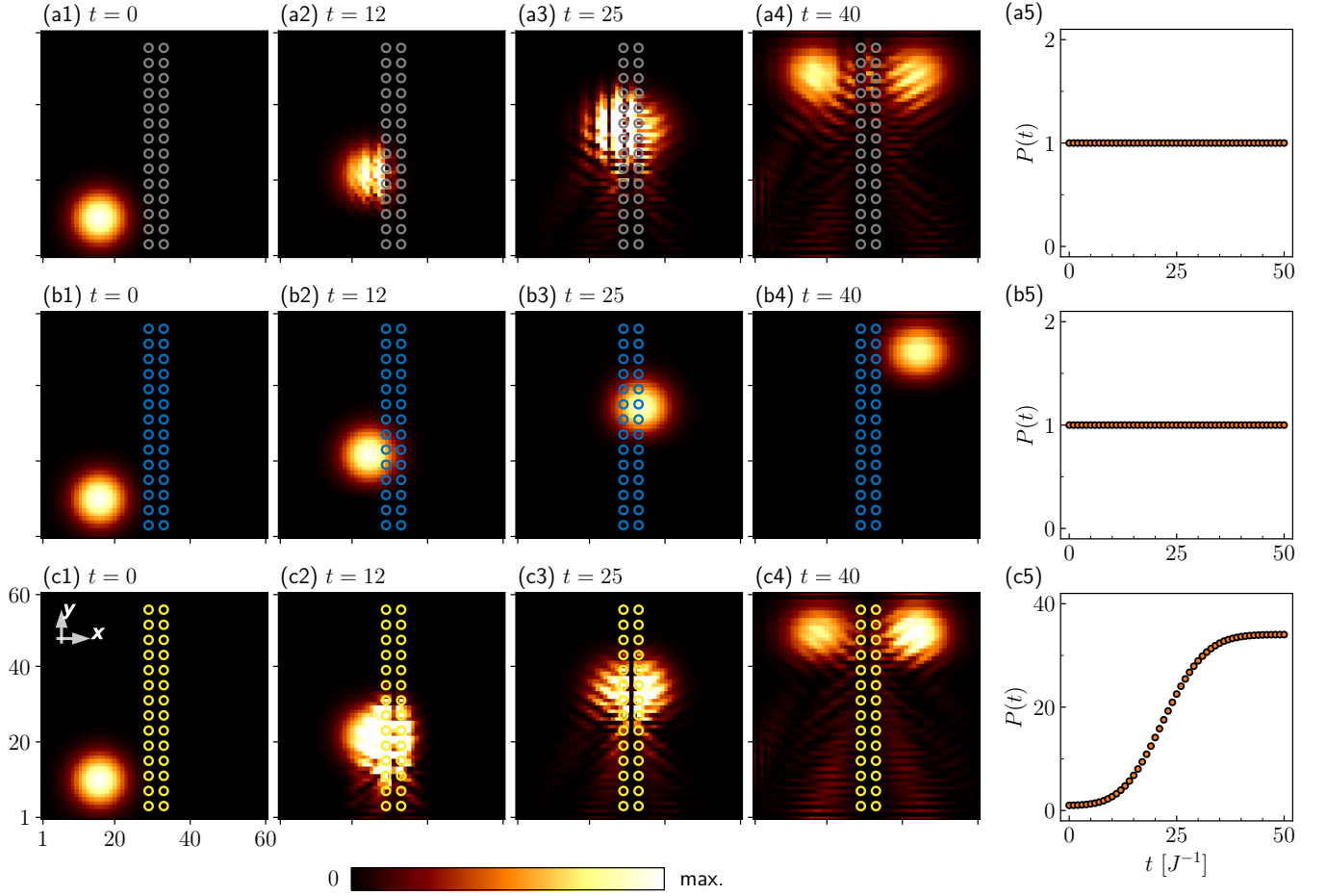


FIG. 3. Bragg scattering in Hermitian 2D system [(a1)-(a5)]. Invisible Bragg scattering [(b1)-(b5)], and amplified Bragg scattering [(c1)-(c5)] in non-Hermitian 2D systems. The left panels are snapshots of intensity $I_{j,l}(t)$ defined in Eq. (16) for the three systems, and the gray, blue and yellow circles represent real field \mathbf{B} , complex fields \mathbf{B}_+ and \mathbf{B}_- , respectively. To better illustrate the Bragg scattering, we take different maximum value of the colorbars at different times. The right panels are the total Dirac probabilities $P(t)$ as functions of time. The parameters of the system are $\kappa = 1$, $|B| = 5$ and $N_x = N_y = 60$, and for the initial excitation are $\alpha = 0.15$, $(j^c, l^c) = (15, 10)$, and $(k_x^c, k_y^c) = (-\pi/4, -\sqrt{3}\pi/4)$. The lattice constant of the Hermitian square lattice is 1, and the distance between impurities is taken as $d = 4$. Here the scale of the Hamiltonian is taken as $J = 2$. One can see that cases (a) and (c) have the same scattering pattern, except the amplification in the latter.

and (k_x^c, k_y^c) is the central momentum. According to the Bragg's law⁴³, the incident wave packet with certain direction $\theta = \arcsin[n\pi/(|\mathbf{k}^c|d)]$ (angle between incident direction and y -axis) will induce constructive interference in the direction of specular reflection. Here n is a positive integer; $|\mathbf{k}^c| = \sqrt{(k_x^c)^2 + (k_y^c)^2}$; and d is the distance between two arrays. We set $n = 1$, $d = 4$, and $|\mathbf{k}^c| = \pi/2$, and perform the numerical simulation of the time evolution $|\Psi(t)\rangle = e^{-iHt} |\Psi(0)\rangle$ by exact diagonalization. The dynamics can be observed through the density distribution in real space defined as

$$I_{j,l}(t) = \sum_{\sigma=\uparrow,\downarrow} |\langle \text{Vac} | c_{j,l,\sigma} | \Psi(t) \rangle|^2, \quad (16)$$

as well as the total Dirac probability

$$P(t) = \sum_{j=1}^{N_x} \sum_{l=1}^{N_y} I_{j,l}(t). \quad (17)$$

The numerical results of $I_{j,l}(t)$ and $P(t)$ are presented in Figs. 3(a1)-(a5). A "Bragg peak" arises in the direction of specular reflection when time $t = 40$, and of course, the Dirac probability is conservative.

Then we turn to the non-Hermitian systems. There are four configurations of the superlattices composed of two parallel EP-impurity arrays: (i) both arrays composed of field \mathbf{B}_+ ; (ii) both arrays composed of field \mathbf{B}_- ; (iii) one array composed of field \mathbf{B}_+ and the other composed of field \mathbf{B}_- ; and (iv) staggered fields \mathbf{B}_\pm form two arrays. Here the complex field is $\mathbf{B}_\pm =$

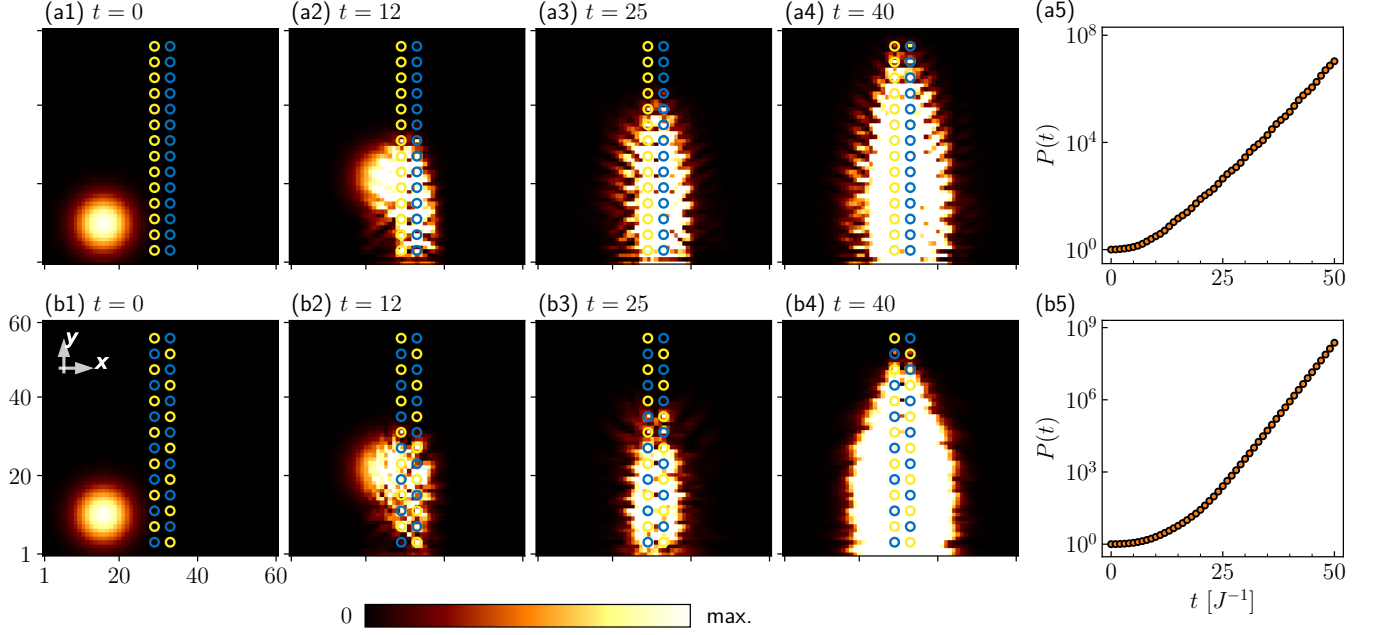


FIG. 4. Resonant mutual stimulation in non-Hermitian 2D systems in case (iii) [(a1)-(a5)] and case (iv) [(b1)-(b5)]. The left panels are snapshots of intensity $I_{j,l}(t)$ defined in Eq. (16) for the two systems, and blue and yellow circles represent complex fields \mathbf{B}_+ and \mathbf{B}_- , respectively. The right panels are the total Dirac probabilities $P(t)$ as functions of time with logarithmic y -axis. Parameters for the both systems and the initial excitation are taken the same as that in Fig. 3, except the configurations of EP-impurity fields. It indicates that the probability in (b) is one order higher than that in (a).

$|B|(1, 0, \pm i)$. The site state with fixed spin polarization $\frac{1}{\sqrt{2}} \left(c_{j,l,\uparrow}^\dagger - i c_{j,l,\downarrow}^\dagger \right) |\text{Vac}\rangle$ in the initial excitation $|\Psi(0)\rangle$ is auxiliary mode of term $\mathbf{B}_- \cdot \mathbf{s}_{j,l}$ and EP mode of term $\mathbf{B}_+ \cdot \mathbf{s}_{j,l}$. Taking the same system parameters (except the impurity fields) and initial excitation as the above Hermitian case, the numerical simulations of the time evolutions are performed. Figs. 3(b1)-(b5) indicate that the superlattice in case (i) is invisible for the evolved state, and the Dirac probability is conservative. Figs. 3(c1)-(c5) indicate that the evolved state in system of case (ii) has the same scattering pattern as case (i), except the amplification: the Dirac probability as function of time is a step-like function. These numerical results verify our prediction and are in accord with the scattering solution of the 1D system H_{scatt} in the previous section.

In view of the mechanism of positive-feedback loop, if two kinds of EP-impurity are both involve in the system, the dynamics of resonant mutual stimulation are expected to be observed. Cases (iii) and (iv) are for this consideration, and the results are plotted in Figs. 4(a1)-(a5) and Figs. 4(b1)-(b5), respectively. In both cases, the dynamics of resonant mutual stimulation is evident, and the Dirac probability as function of time is exponential after the wave packet being scattered by the EP-impurity arrays. Clearly, the Dirac probability increases more rapidly for the latter case, due to the sufficient mixing of two kinds of EP-impurities.

V. SUMMARY

In summary, we have developed a theory for a class of non-Hermitian Hamiltonian which supports a special dynamics due to the coexistence of coalescing and zero modes. The most fascinating and important feature of such systems is the resonant mutual stimulation. As an example, we have investigate the dynamics of a non-Hermitian spin- $\frac{1}{2}$ fermionic tight-binding model. It is shown that a pair of conjugate EP modes can act as a resonant amplifier since its equivalent Hamiltonian is a positive-feedback loop. The resonant tunneling between coalescing and zero modes allows the construction of superlattice, in which non-Hermitian EP-impurity array is embedded in Hermitian lattice as substrate. We demonstrate the EP spintronics based on numerical simulations, including resonant amplification and invisibility of Bragg fringe. Our findings offer a platform for non-Hermitian spin devices.

ACKNOWLEDGMENTS

This work was supported by the National Natural Science Foundation of China (under Grant No. 11874225).

APPENDIX

In this Appendix, we consider a class of non-Hermitian Hamiltonian which supports a special dynamics. The model Hamiltonian in Eq. (1) we study in this paper is one of examples in this class. In general, the Hamiltonian we concern reads as follows

$$\begin{aligned} H &= \sum_{j < l} H_{jl} + \sum_{j=1}^N H_j, \\ H_{jl} &= \kappa_{jl} \sum_{\alpha=1}^{N_{\text{clust}}} a_{j,\alpha}^\dagger a_{l,\alpha} + \text{H.c.}, \\ H_j &= B_j \sum_{\alpha,\beta=1}^{N_{\text{clust}}} J_{\alpha\beta} a_{j,\alpha}^\dagger a_{j,\beta}, \end{aligned} \quad (\text{A1})$$

which consists of N isomorphic clusters H_j , with each cluster has a dimension N_{clust} . The label j denotes the j th subgraph of N clusters, and $a_{j,\alpha}^\dagger$ ($a_{j,\alpha}$) is the boson or fermion creation (annihilation) operator at the α th site in the j th cluster. The cluster H_j is defined by the distribution of the hopping integrals $\{B_j J_{\alpha\beta}\}$ where the parameter B_j is real, while the matrix $J_{\alpha\beta}$ is not Hermitian. All H_j have the same eigenstates and spectral structures due to the fact that the geometry of each cluster is isomorphic. Meanwhile terms $\sum_{j < l} H_{jl}$ is self-adjoint, i.e., $H_{jl} = H_{jl}^\dagger$, which describes the Hermitian connection between clusters. And such kind of couplings are the type of similarity mapping, which is crucial for features in the dynamics of the Hamiltonian H .

1. Pseudo-Hermitian modes

Firstly, we consider the case of H_j being pseudo-Hermitian, i.e., H_j is non-Hermitian but can be diagonalized in the context of biorthonormal inner product. Following the well established pseudo-Hermitian quantum mechanics^{2,44–46}, we always have

$$H_j = B_j \sum_{\lambda=1}^{N_{\text{clust}}} \varepsilon_\lambda \bar{d}_{j,\lambda} d_{j,\lambda}, \quad (\text{A2})$$

with the operators $\bar{d}_{j,\lambda}$ and $d_{j,\lambda}$ being defined as

$$\bar{d}_{j,\lambda} = \sum_{\alpha=1}^{N_{\text{clust}}} h_{\alpha\lambda} a_{j,\alpha}^\dagger, \quad d_{j,\lambda} = \sum_{\alpha=1}^{N_{\text{clust}}} g_{\alpha\lambda}^* a_{j,\alpha}, \quad (\text{A3})$$

where

$$\sum_{\lambda=1}^{N_{\text{clust}}} g_{\alpha\lambda}^* h_{\lambda\alpha'} = \delta_{\alpha\alpha'}. \quad (\text{A4})$$

Here the existence of biorthogonal complete set of $\{g_{\alpha\lambda}, h_{\alpha\lambda}\}$ rules out the exceptional point, which will be

discussed in the next section. Note that $\{g_{\alpha\lambda}\}$, $\{h_{\alpha\lambda}\}$ and $\{\varepsilon_\lambda\}$ are independent of the index j . Then the operators $\bar{d}_{j,\lambda}$ and $d_{j,\lambda}$ are canonical conjugate pairs, satisfying

$$\begin{aligned} [d_{j,\lambda}, \bar{d}_{j',\lambda'}]_\pm &= \delta_{jj'} \delta_{\lambda\lambda'}, \\ [d_{j,\lambda}, d_{j',\lambda'}]_\pm &= [\bar{d}_{j,\lambda}, \bar{d}_{j',\lambda'}]_\pm = 0, \end{aligned} \quad (\text{A5})$$

where $[\dots]_\pm$ denotes the commutator and anti-commutator, depending on whether the excitation of the model is boson or fermion.

And accordingly, the original Hamiltonian can be rewritten as the form

$$H = \sum_{\lambda=1}^{N_{\text{clust}}} H^\lambda, \quad (\text{A6})$$

where the sub-Hamiltonian is

$$H^\lambda = \varepsilon_\lambda \sum_{j=1}^N B_j \bar{d}_{j,\lambda} d_{j,\lambda} + \sum_{j < l} (\kappa_{jl} \bar{d}_{j,\lambda} d_{l,\lambda} + \kappa_{jl}^* \bar{d}_{l,\lambda} d_{j,\lambda}). \quad (\text{A7})$$

The relations

$$[H^\lambda, H^{\lambda'}] = 0, \quad (\text{A8})$$

indicates that the existence of invariant subspace indexed by λ . When a given eigenvalue ε_λ is real, the dynamics in the corresponding invariant subspace obeys the conservation of Dirac probability⁴⁷.

2. Coalescing and zero modes

We then consider the system, which is consisted of two types of clusters with zero eigenvalue: (i) being in EP and (ii) with $B_j = 0$, respectively. We denote the coalescing mode of cluster j at EP as $(\bar{d}_{j,C}, d_{j,C})$, i.e.,

$$H_j = B_j \sum_{\lambda=1, \lambda \neq C}^{N_{\text{clust}}-2} \varepsilon_\lambda \bar{d}_{j,\lambda} d_{j,\lambda} + 0 \times \bar{d}_{j,C} d_{j,C}. \quad (\text{A9})$$

Here, there are total $N_{\text{clust}} - 1$ modes, with an auxiliary mode $(\bar{d}_{j,A}, d_{j,A})$ being ruled out. For a cluster with $B_j = 0$, it has N_{clust} -fold degenerate modes with zero eigenvalue. One of them can be $(\bar{d}_{j,C}, d_{j,C})$ or its auxiliary mode $(\bar{d}_{j,A}, d_{j,A})$. The total Hamiltonian H hence possesses the common EP as H_j . When multi-non-Hermitian clusters are involved, H supports high-order EP.

Now we consider the Hamiltonian in invariant subspace spanned by coalescing mode, which has the form

$$H^C = \sum_{j < l} (\kappa_{jl} \bar{d}_{j,C} d_{l,C} + \kappa_{jl}^* \bar{d}_{l,C} d_{j,C}). \quad (\text{A10})$$

It acts as a Hermitian Hamiltonian and exhibits Dirac probability preserving dynamics. On the other hand, for

the auxiliary mode, the inter-cluster dynamics can still obey the Hamiltonian

$$H^A = \sum_{j < l} (\kappa_{jl} \bar{d}_{j,A} d_{l,A} + \kappa_{jl}^* \bar{d}_{l,A} d_{j,A}). \quad (\text{A11})$$

However, the dynamics of an inner non-Hermitian cluster obeys the non-Hermitian quantum mechanics, violating the conservation of Dirac probability. In summary, if the initial state only involves the coalescing mode, it will evolve in Hermitian manner, while blow up the probability for auxiliary mode. In the main text, the example with $N_{\text{clust}} = 2$ demonstrates this point in detail.

-
- * songtc@nankai.edu.cn
- ¹ I. Žutić, J. Fabian, and S. Das Sarma, “Spintronics: Fundamentals and applications,” *Rev. Mod. Phys.* **76**, 323–410 (2004).
 - ² C. M Bender, “Making sense of non-hermitian hamiltonians,” *Rep. Prog. Phys.* **70**, 947 (2007).
 - ³ N. Moiseyev, *Non-Hermitian quantum mechanics* (Cambridge University Press, 2011).
 - ⁴ A. Krasnok, D. Baranov, H. Li, M.-A. Miri, F. Monticone, and A. Alú, “Anomalies in light scattering,” *Adv. Opt. Photonics* **11**, 892–951 (2019).
 - ⁵ L. Feng, Y.-L. Xu, W. S Fegadolli, M.-H. Lu, J. EB Oliveira, V. R Almeida, Y.-F. Chen, and A. Scherer, “Experimental demonstration of a unidirectional reflectionless parity-time metamaterial at optical frequencies,” *Nat. Mater.* **12**, 108–113 (2013).
 - ⁶ S. K. Gupta, Y. Zou, X.-Y. Zhu, M.-H. Lu, L.-J. Zhang, X.-P. Liu, and Yan-Feng Chen, “Parity-time symmetry in non-hermitian complex optical media,” *Adv. Mater.* , 1903639 (2019).
 - ⁷ A. Guo, GJ Salamo, D. Duchesne, R. Morandotti, M. Volatier-Ravat, V. Aimez, GA Siviloglou, and D. N Christodoulides, “Observation of p t-symmetry breaking in complex optical potentials,” *Phys. Rev. Lett.* **103**, 093902 (2009).
 - ⁸ C. E Rüter, K. G Makris, R. El-Ganainy, D. N Christodoulides, M. Segev, and D. Kip, “Observation of parity-time symmetry in optics,” *Nat. Phys.* **6**, 192–195 (2010).
 - ⁹ B. Peng, Ş. K. Özdemir, F. Lei, F. Monifi, M. Gianfreda, G. L. Long, S. Fan, F. Nori, C. M Bender, and L. Yang, “Parity-time-symmetric whispering-gallery microcavities,” *Nat. Phys.* **10**, 394–398 (2014).
 - ¹⁰ L. Feng, Z. J. Wong, R.-M. Ma, Y. Wang, and X. Zhang, “Single-mode laser by parity-time symmetry breaking,” *Science* **346**, 972–975 (2014).
 - ¹¹ H. Hodaei, M.-A. Miri, M. Heinrich, D. N Christodoulides, and M. Khajavikhan, “Parity-time-symmetric microring lasers,” *Science* **346**, 975–978 (2014).
 - ¹² L. Feng, R. El-Ganainy, and L. Ge, “Non-hermitian photonics based on parity-time symmetry,” *Nat. Photon.* **11**, 752–762 (2017).
 - ¹³ S. Longhi, “Parity-time symmetry meets photonics: A new twist in non-hermitian optics,” *Eur. Phys. Lett.* **120**, 64001 (2018).
 - ¹⁴ R. El-Ganainy, K. G Makris, M. Khajavikhan, Z. H Muslimani, S. Rotter, and D. N Christodoulides, “Non-hermitian physics and pt symmetry,” *Nat. Phys.* **14**, 11–19 (2018).
 - ¹⁵ M.-A. Miri and A. Alú, “Exceptional points in optics and photonics,” *Science* **363**, eaar7709 (2019).
 - ¹⁶ ŞK Özdemir, S. Rotter, F. Nori, and L. Yang, “Parity-time symmetry and exceptional points in photonics,” *Nat. Mater.* **18**, 783–798 (2019).
 - ¹⁷ Y. Wu, W. Liu, J. Geng, X. Song, X. Ye, C.-K. Duan, X. Rong, and J. Du, “Observation of parity-time symmetry breaking in a single-spin system,” *Science* **364**, 878–880 (2019).
 - ¹⁸ S. Klaiman, U. Günther, and N. Moiseyev, “Visualization of branch points in p t-symmetric waveguides,” *Phys. Rev. Lett.* **101**, 080402 (2008).
 - ¹⁹ J. Doppler, A. A Mailybaev, J. Böhm, U. Kuhl, A. Girschik, F. Libisch, T. J Milburn, P. Rabl, N. Moiseyev, and S. Rotter, “Dynamically encircling an exceptional point for asymmetric mode switching,” *Nature* **537**, 76–79 (2016).
 - ²⁰ H. Xu, D. Mason, L. Jiang, and JGE Harris, “Topological energy transfer in an optomechanical system with exceptional points,” *Nature* **537**, 80–83 (2016).
 - ²¹ S. Assaworrorarit, X. Yu, and S. Fan, “Robust wireless power transfer using a nonlinear parity-time-symmetric circuit,” *Nature* **546**, 387–390 (2017).
 - ²² B. Midya, H. Zhao, and L. Feng, “Non-hermitian photonics promises exceptional topology of light,” *Nat. Commun.* **9**, 1–4 (2018).
 - ²³ S. Cao and Z. Hou, “Angular-asymmetric transmitting metasurface and splitter for acoustic waves: Combining the coherent perfect absorber and a laser,” *Phys. Rev. Applied* **12**, 064016 (2019).
 - ²⁴ P. Miao, Z. Zhang, J. Sun, W. Walasik, S. Longhi, N. M Litchinitser, and L. Feng, “Orbital angular momentum microlaser,” *Science* **353**, 464–467 (2016).
 - ²⁵ S. Longhi and L. Feng, “Unidirectional lasing in semiconductor microring lasers at an exceptional point,” *Photon. Res.* **5**, B1–B6 (2017).
 - ²⁶ W. Chen, Ş. K. Özdemir, G. Zhao, J. Wiersig, and L. Yang, “Exceptional points enhance sensing in an optical microcavity,” *Nature* **548**, 192–196 (2017).
 - ²⁷ H. Hodaei, A. U Hassan, S. Wittek, H. Garcia-Gracia, R. El-Ganainy, D. N Christodoulides, and M. Khajavikhan, “Enhanced sensitivity at higher-order exceptional points,” *Nature* **548**, 187–191 (2017).
 - ²⁸ J. Wiersig, “Enhancing the sensitivity of frequency and energy splitting detection by using exceptional points: application to microcavity sensors for single-particle detection,” *Phys. Rev. Lett.* **112**, 203901 (2014).
 - ²⁹ M. Am-Shallem, R. Kosloff, and N. Moiseyev, “Parameter estimation in atomic spectroscopy using exceptional points,” *Phys. Rev. A* **93**, 032116 (2016).
 - ³⁰ Z.-P. Liu, J. Zhang, Ş. K. Özdemir, B. Peng, H. Jing, X.-Y. Lü, C.-W. Li, L. Yang, F. Nori, and Y.-x. Liu, “Metrology with pt-symmetric cavities: enhanced sensitivity near the pt-phase transition,” *Phys. Rev. Lett.* **117**, 110802 (2016).
 - ³¹ H.-K. Lau and A. A Clerk, “Fundamental limits and non-

- reciprocal approaches in non-hermitian quantum sensing,” *Nat. Commun.* **9**, 1–13 (2018).
- ³² M. Zhang, W. Sweeney, C. W. Hsu, L. Yang, AD Stone, and L. Jiang, “Quantum noise theory of exceptional point amplifying sensors,” *Phys. Rev. Lett.* **123**, 180501 (2019).
- ³³ P. Djorwe, Y. Pennec, and B. Djafari-Rouhani, “Exceptional point enhances sensitivity of optomechanical mass sensors,” *Phys. Rev. Applied* **12**, 024002 (2019).
- ³⁴ Y.-H. Lai, Y.-K. Lu, M.-G. Suh, Z. Yuan, and K. Vahala, “Observation of the exceptional-point-enhanced sagnac effect,” *Nature* **576**, 65–69 (2019).
- ³⁵ M. P Hokmabadi, A. Schumer, D. N Christodoulides, and M. Khajavikhan, “Non-hermitian ring laser gyroscopes with enhanced sagnac sensitivity,” *Nature* **576**, 70–74 (2019).
- ³⁶ Y. Cao and P. Yan, “Exceptional magnetic sensitivity of p t-symmetric cavity magnon polaritons,” *Phys. Rev. B* **99**, 214415 (2019).
- ³⁷ G.-Q. Zhang, Y.-P. Wang, and JQ You, “Dispersive readout of a weakly coupled qubit via the parity-time-symmetric phase transition,” *Phys. Rev. A* **99**, 052341 (2019).
- ³⁸ C. Chen, L. Jin, and R.-B. Liu, “Sensitivity of parameter estimation near the exceptional point of a non-hermitian system,” *New J. Phys.* **21**, 083002 (2019).
- ³⁹ X. Z. Zhang, L. Jin, and Z. Song, “Self-sustained emission in semi-infinite non-hermitian systems at the exceptional point,” *Phys. Rev. A* **87**, 042118 (2013).
- ⁴⁰ P. Wang, L. Jin, G. Zhang, and Z. Song, “Wave emission and absorption at spectral singularities,” *Phys. Rev. A* **94**, 053834 (2016).
- ⁴¹ X. M. Yang, X. Z. Zhang, C. Li, and Z. Song, “Dynamical signature of the moiré pattern in a non-hermitian ladder,” *Phys. Rev. B* **98**, 085306 (2018).
- ⁴² T. E. Lee and C.-K. Chan, “Heralded magnetism in non-hermitian atomic systems,” *Phys. Rev. X* **4**, 041001 (2014).
- ⁴³ W. H. Bragg and W. L. Bragg, “The reflection of x-rays by crystals,” *Proc. R. Soc. Lond. A* **88**, 428–438 (1913).
- ⁴⁴ P. Dorey, C. Dunning, and R. Tateo, “The ode/im correspondence,” *J. Phys. A: Math. Theor.* **40**, R205 (2007).
- ⁴⁵ A. Mostafazadeh, “Pseudo-hermitian representation of quantum mechanics,” *Int. J. Geom. Meth. Mod. Phys.* **7**, 1191–1306 (2010).
- ⁴⁶ L. Jin and Z. Song, “Scaling behavior and phase diagram of a pt-symmetric non-hermitian bose–hubbard system,” *Ann. Phys.* **330**, 142–159 (2013).
- ⁴⁷ L. Jin and Z. Song, “Hermitian dynamics in a class of pseudo-hermitian networks,” *Phys. Rev. A* **84**, 042116 (2011).